A marked point process model with strong prior shape information for the extraction of multiple, arbitrarily-shaped objects

Maria Kulikova, Ian Jermyn,
Xavier Descombes, and Josiane Zerubia
Ariana research team
INRIA Sophia-Antipolis Mediterannee
2004 route des Lucioles
06902 Sophia-Antipolis, Cedex France
Email: {name.surname@inria.fr}

Elena Zhizhina
Dobroushin's Laboratory of Mathematics
Institute of Information Transmission Problems (IITP)
Bolshoy Karetny per. 19
127994 Moscow, Russia
Email: ejj@iitp.ru

Abstract—We define a method for incorporating strong prior shape information into a recently extended Markov point process model for the extraction of arbitrarily-shaped objects from images. To estimate the optimal configuration of objects, the process is sampled using a Markov chain based on a stochastic birth-and-death process defined in a space of multiple objects. The single objects considered are defined by both the image data and the prior information in a way that controls the computational complexity of the estimation problem. The method is tested via experiments on a very high resolution aerial image of a scene composed of tree crowns.

I. INTRODUCTION

Object detection from optical satellite and aerial images is one of the most important tasks in remote sensing image analysis. The problem arises in many applications, both civilian and military, *e.g.* tree counting and species classification for biomass or biodiversity estimation; and bird counting for monitoring population changes. Nowadays the resolution of aerial images is approaching a few centimetres. At this level of resolution, the geometry of objects is clearly visible, and needs to be taken into account for accurate object extraction.

Stochastic point process models are known for their ability to include this type of information. A probability distribution is defined on the space of configurations composed of multiple objects which depends on the relation between the objects and data, and on the configuration of individual objects as well as their joint relations. The extracted objects are then those in the 'optimal' configuration, which is usually estimated using maximum a priori (MAP) estimation.

In previous work, marked point process (MPP) models have been used for the extraction of road networks [11], buildings [13] and trees [15], from images of more than 50 cm/pixel resolution. At that level the objects have a simplified geometrical shape and were thus represented using simple shape objects, *e.g.* discs, ellipses, or rectangles.

Recently we lifted this restriction without increasing the dimension of the space of a single object [10]. A single object was represented by its boundary, a closed curve, but the set of possible single objects (*i.e.* boundaries) was defined not *a priori*, but by the image data and a single-object version of the model. A probability distribution was then defined on the configuration space of an unknown number of objects.

This approach is well suited to scenes composed of objects that do not vary too much in shape and size within a class, and that have smooth enough boundaries. In this case, accuracy in the number of extracted objects can be achieved by favouring the smoothness term that controls, as well, the length of the curve. The model can thus to some degree separate objects that overlap, but this leads to imprecision in delineating objects.

The aim of this paper is to incorporate into the single-object model, prior knowledge about the shape of the objects sought, in order to deal with overlapping objects with complex shapes without losing their geometric details and without significantly increasing the computational complexity of estimation.

Our work can also be viewed as an extension of the active contour methodology [8] to cases in which the number of objects is unknown *a priori*, and where shape prior information is incorporated as well. Much work has been already done based on the active contour approach. Some of this work, *e.g.* [1], includes only weak shape information, essentially smoothness, but can in principle detect multiple (although not overlapping) objects using the level set representation [14], [16]. Other work includes much stronger prior information about shape [2], [4], [6], [12], but the method used to do this means that it is difficult to treat an unknown number of objects (and in practice only single objects are treated). Cremers *et al.* [3] treat the problem of image segmentation into connected components each of which corresponds to one class of a number of distinct classes of objects, but only one object can be found in each connected component.

Additionally, the results obtained by these methods may be very dependent on the initial configuration, since the algorithm typically used is deterministic gradient descent. Storvik [18] and Juan *et al.* [7] respectively use an Markov Chain Monte Carlo (MCMC) approach and stochastic partial differential

equations (SPDEs) optimization techniques to minimize active contour energies, but the algorithms make only local changes to the contour at each iteration, and thus preserve object number. Srivastava and Jermyn [17] use a stochastic algorithm together with an energy including strong prior shape information for the extraction and classification of objects from 2D point clouds, but only a single object is sought. Tu *et al.* [19] use data-driven reversible jump Markov Chain Monte Carlo (RJMCMC) dynamics to solve a problem of general purpose image segmentation, but our work differs, first, in addressing a specific problem rather than general possibilities; and second, in using birth-and-death rather than RJMCMC dynamics. The advantage of birth-and-death dynamics is their faster convergence, due to the fact that at each iteration, several objects are simultaneously added to the current configuration without any rejection probability.

The remainder of the article is organized as follows. In section II, we describe the single-object space and the single-object term in the energy function. In section III, we describe the multiple-object space and the full energy. In the same section, we describe the sampling and estimation algorithm. In section IV, we present experimental results, and in section V we conclude.

II. SINGLE-OBJECTS

As mentioned, the single-object space will not be determined *a priori* to consist of simple geometrical shapes, but rather will be constructed using the image data and a model describing configurations of individual objects. We model individual object boundaries as closed planar curves $\gamma : [0, 2\pi] \rightarrow V \subset \mathbb{R}^2$ lying in the image domain V. The set of closed curves we will consider here consists of 'star domains' parameterized by $(x_0, \delta r(t))$, where $x_0 \in \mathbb{R}^2$ and $\delta r : [0, 2\pi] \rightarrow \mathbb{R}$ is a radial variation around a circle $\gamma_c(t)$ of radius $r_0 \in [r_{\min}, r_{\max}]$ centred at $x_0 \in V$, where $t \in [0, 2\pi]$. Then,

$$\gamma(t) = x_0 + \gamma_c(t) + \delta\gamma(t) , \qquad (1)$$

where $\delta\gamma$ is the radial variation expressed in Euclidean coordinates. More explicitly,

$$
\begin{aligned}
\gamma(t) &= x_0 + ((r_0 + \delta r(t))\cos\theta_c(t), (r_0 + \delta_r(t))\sin\theta_c(t)) \\
&= (x_0^x, x_0^y) + (r_0 + \delta r(t))(\cos(t), \sin(t)) .
\end{aligned}
$$

We suppose that we are given an energy function E defined on a space Γ of these curves (with appropriate restrictions to ensure that everything is well-defined). This energy function will depend on the image data also, as it will be detailed below in the article.

Given an initial curve $\gamma \in \Gamma$, we can then perform gradient descent to arrive at a local minimum of E, giving a second curve, $\tilde{\gamma} \in \Gamma$. The map $\tilde{\cdot} : \Gamma \rightarrow \Gamma$ takes every curve to the local minimum in whose basin of attraction it lies. Now define the space $\mathcal{C}$ to be a set of circles lying in the image domain, with radii $r_0 \in [r_{\min}, r_{\max}]$, parameterized by arc length. The single-object space we consider is $\Gamma_o = \tilde{\mathcal{C}}$. The possible single objects are thus locally adapted to the data. Then despite

allowing for potentially arbitrarily shaped star domains, the dimension of the single-object space remains small: if we fix the centre of the circle in $\mathcal{C}$, *i.e.* the 'point' in the marked point process, the 'mark' is one-dimensional, being equivalent to the circle's radius.

A. Single-object energy

To define the space Γ_o, we have to define the energy E. In this paper, we define it as a sum of two terms: a term related to the curve, *i.e.* a prior term, and an image term, also called the data term:

$$E(\gamma(t)) = E_{\text{image}}(\gamma(t)) + E_{\text{curve}}(\gamma(t)) . \qquad (2)$$

The image energy term is defined as a weighted sum:

$$
\begin{aligned}
E_{\text{image}}(\gamma) \quad = \quad & \lambda_g \int_{[0,2\pi]} dt \, n(t) \cdot \nabla I(\gamma(t)) \qquad (3) \\
& + \lambda_G \int_{R(\gamma)} d^2x \, (G(x) - \bar{G}(x)) ,
\end{aligned}
$$

where $n(t)$ is the (unnormalized) outward normal to the curve; I is the image; $G(x) = \frac{(I(x)-\mu)^2}{2\sigma^2}$ and $\bar{G}(x) = \frac{(I(x)-\bar{\mu})^2}{2\bar{\sigma}^2}$; and $R(\gamma)$ is the interior region corresponding to the boundary γ. The first term favours boundaries with high image gradients normal to the boundary. The second term arises from a Gaussian image model with different means and variances for the interior and exterior of the objects. Both terms are negative where $\gamma(t)$ is well-adapted to the data. The parameters μ, σ, and $\bar{\mu}$, $\bar{\sigma}$, are learned from examples of object and background.

We define $E_{\text{curve}}(t)$ as a sum of two terms:

$$E_{\text{curve}}(\gamma(t)) = E_{\text{smth}}(\gamma(t)) + E_{\text{sh}}(\gamma(t)) , \qquad (4)$$

We show below that it can be written in the following form:

$$E_{\text{curve}}(\gamma(t)) = \iint_{[0,2\pi]} dt dt' \, F(t - t')\delta r(t)\delta r(t') . \qquad (5)$$

The $E_{\text{smth}}(\gamma)$ term favours boundary smoothness and a uniform parametrization of the curve:

$$E_{\text{smth}}(\gamma) = \int_{[0,2\pi]} dt \, |\dot{\gamma}(t)|^2 , \qquad (6)$$

where $\dot{\gamma}$ is the derivative of γ. The second term $E_{\text{sh}}(\gamma)$ represents the prior energy associated with the curve shape. It is a quadratic function of δr, which due to invariance to translations of the origin of the curve, is diagonal in the Fourier basis on the circle, and has zero mean except at zero frequency. The latter correspond to changes in radius, and are absorbed in r_0. The energy is thus defined by the variance of each Fourier component, $\sigma(k)^2 = \frac{1}{2g(k)}$. The function $g(k)$ restricts or favours perturbations of the circle with different frequencies k, thereby reflecting the specificities of the shapes of the objects to be detected in the image:

$$E_{\text{sh}}(\gamma) = 2\pi \sum_{k \in \mathbb{Z}} g(k)|\hat{\delta r}(k)|^2 ,$$

where

$$\hat{\delta r}(k) = \frac{1}{2\pi} \int_{[0,2\pi]} dt \exp(-ikt)\delta r(t) . \qquad (7)$$

Notice that for our parameterized set of curves, $|\dot{\gamma}(t)|^2 = \dot{\delta r}(t)^2 + (r_0 + \delta r(t))^2$, so that $E_{\text{smth}}(\gamma)$ can be written in following way:

$$E_{\text{smth}}(\gamma) = \int_{[0,2\pi]} dt \, (\dot{\delta r}(t)^2 + (r_0 + \delta r(t))^2)$$
$$= 2\pi \left(\sum_{k \in \mathbb{Z}} (k^2 + 1)|\hat{\delta r}(k)|^2 + 2r_0 \hat{\delta r}(0) + r_0^2 \right) .$$

Thus, the prior energy E_{curve} takes the form:

$$E_{\text{curve}}(\gamma) = 2\pi \sum_{k \in \mathbb{Z}} (k^2 + 1 + g(k))|\hat{\delta r}(k)|^2$$
$$+ 2\pi 2r_0 \hat{\delta r}(0) + 2\pi r_0^2 .$$

Defining a function $f(k) = k^2 + 1 + g(k)$, and dropping both $\frac{1}{\pi} r_0^2$, which is simply an additive constant, and the linear term $\frac{1}{\pi} r_0 \hat{\delta r}(0)$, which serves only to change the mean of $\hat{\delta r}(0)$, which we define to be zero, we can write:

$$E_{\text{curve}}(\gamma) = 2\pi \sum_{k \in \mathbb{Z}} f(k)|\hat{\delta r}(k)|^2 . \tag{8}$$

Now using the inverse Fourier Transform of $f(k)$ and taking into account equation (7), equation (8) can be written as

$$E_{\text{curve}}(\gamma) = \frac{1}{2\pi} \sum_{k \in \mathbb{Z}} f(k) \iint_{[0,2\pi]} dt dt' e^{ikt} e^{-ikt'} \delta r(t) \delta r(t')$$
$$= \frac{1}{2\pi} \iint_{[0,2\pi]} dt dt' \delta r(t) \delta r(t') \sum_{k \in \mathbb{Z}} e^{ik(t-t')} f(k)$$
$$= \frac{1}{2\pi} \iint_{[0,2\pi]} dt dt' \delta r(t) \delta r(t') F(t - t') .$$

Thus we obtain equation (5) where

$$F(t - t') = \sum_{k \in \mathbb{Z}} \exp ik(t - t') f(k) .$$

The algorithm makes uses of the functional derivative of E:

$$\frac{\delta E}{\delta \gamma(t)} = \left(\frac{\partial E}{\partial x_0(\gamma(t))}, \frac{\delta E}{\delta \delta r(\gamma(t))} \right) , \tag{9}$$

where the components taking the following forms:

$$\frac{\partial E}{\partial x_0^i(\gamma(t))} = \int_{[0,2\pi]} dt (-n(\gamma(t))) \cdot \partial_i \nabla I(\gamma(t))$$
$$+ \int_{[0,2\pi]} dt (-n(\gamma(t))) \cdot \partial_i u(\gamma(t)) ,$$

with u a vector field satisfying $\nabla \cdot u = (G - \bar{G})$ and i indexing Euclidean coordinates on $\mathbb{R}^2$; and

$$\frac{\delta E}{\delta \delta r(t)} = \lambda_g (r_0 + \delta r(t)) \nabla^2 I(\gamma(t))$$
$$+ \lambda_G (r_0 + \delta r(t))(G - \bar{G})(\gamma(t))$$
$$+ \frac{1}{\pi} \int_{[0,2\pi]} dt' F(t - t') \delta r(t') .$$

III. MULTIPLE OBJECTS: MODEL AND ALGORITHM

The multiple-object space is the "exponential" of the single-object space, *i.e.* it consists of all configurations of zero or more objects:

$$\Omega_{\Gamma_o} = \bigcup_{n=0}^{\infty} \left[\hat{\Gamma}_o^n / S_n \right] , \tag{10}$$

where S_n indicates the symmetric group of n elements acting on the components of the product. Note that the map $\tilde{\cdot}$ extends to a map from $\Omega_{\mathcal{C}}$ (the exponential of $\mathcal{C}$) to Ω_{Γ_o}. Elements of $\Omega_{\mathcal{C}}$ will be denoted ω.

A. Energy

Given a (real, bounded below) function $H(\omega)$ on $\Omega_{\mathcal{C}}$, we define the Gibbs distribution μ_β in terms of the density $p(\omega) = \frac{d\mu_\beta}{d\lambda}(\omega)$ w.r.t. Lebesgue-Poisson measure λ on $\Omega_{\mathcal{C}}$:

$$p(\omega) = \frac{z^{|\omega|}}{Z_\beta} \exp\{-\beta H(\omega)\} , \tag{11}$$

with parameters $\beta > 0$, $z > 0$ and a normalizing factor Z_β:

$$Z_\beta = \int_{\Omega_{\mathcal{C}}} d\lambda(\omega) z^{|\omega|} \exp\{-\beta H(\omega)\} .$$

The energy $H(\omega)$ takes the form:

$$H(\omega) = c_0 \sum_i H_1(\omega_i) + \sum_{i \neq j} H_2(\omega_i, \omega_j) ,$$

where ω_i are the components of ω and c_0 is a weighting parameter. The data term H_1, is defined as

$$H_1(\omega_i) = E(\tilde{\omega}_i) .$$

The term H_2 is the interaction term, which controls the relations between objects, and, in particular discourages overlaps. It is defined as

$$H_2(\omega_i, \omega_j) = \frac{A(R(\tilde{\omega}_i) \cap R(\tilde{\omega}_j))}{\min(A(R(\tilde{\omega}_i)), A(R(\tilde{\omega}_j)))} + \delta_\epsilon(\omega_i, \omega_j) ,$$

where

$$\delta_\epsilon(\omega_i, \omega_j) = \begin{cases} \infty, & |x_0^i - x_0^j| \leq \epsilon; \\ 0, & \text{otherwise,} \end{cases} \tag{12}$$

A is the area functional and δ_ϵ is a hard-core repulsion that prevents two components of ω from coinciding (to some tolerance ϵ). Indeed, if there were no interactions between objects except that they should not coincide, then the optimal configuration of objects would consist of the negative energy elements in Γ_o. The interaction term was thus introduced to prevent the "condensation" of an infinite number of the lowest energy single-object in configuration.

B. Sampling and estimation

In order to estimate the configuration of the objects in the image, we use maximum a posteriori estimation, performed by sampling from the probability distribution μ_β and applying an annealing scheme. The sampling uses a Markov chain in Ω_C consisting of a discrete-time multiple birth-and-death process describing all possible transitions from the configuration ω to the configuration $\omega' \cup \omega''$, where $\omega' \subset \omega$ and ω'' is any new configuration. The transition probabilities of this Markov chain take the form:

$$\mathrm{P}(\omega \to \omega' \cup \omega'') = \prod_{\omega_i' \in \omega'} \frac{1}{1 + \delta d_\beta} \prod_{\omega_i \in \omega \setminus \omega'} \frac{\delta d_\beta}{1 + \delta d_\beta} \times (z\delta)^{|\omega''|} \tag{13}$$

where d_β is the intensity of the death step of the process detailed in section III-C below.

This Markov chain can be considered as an approximation of a continuous-time reversible process and converging to it [5], which, within a logarithmic annealing scheme, guarantees uniform convergence to the measure concentrated on the global minima of the energy function $H(\omega)$.

C. Algorithm description

We define C as the set of circles lying in the image domain V, with radii in the range $[r_{\min}, r_{\max}]$ and with centres at the image pixels. The curves are represented by a chain of points in $\mathbb{R}^2$ defined to correspond to discrete parameter values $t_n = 2\pi n/N$ for $n \in \{0, \dots, (N-1)\}$. The circles in C are assumed to have arc length parametrization, and thus will have equally spaced points.

The birth step of the process adds an unknown number of circles to the current configuration with an intensity z that is independent of the current temperature $T = 1/\beta$. The death step removes a number of components from the current configuration with a probability that depends on the current (inverse) temperature β and the energy difference $\Delta_i H(\omega) = H(\omega \setminus \omega_i) - H(\omega)$. In more detail, the algorithm is as follows:

1) **Initialization**
   Discretisation step $\delta = \delta_0$; inverse temperature $\beta = \beta_0$; Poisson mean z_0; radius range $[r_{\min}, r_{\max}]$; parameters in E;

2) **Birth**
   a) Sample a configuration of circles with radii uniformly distributed on $[r_{\min}, r_{\max}]$, from the Lebesgue-Poisson distribution with intensity $z = \delta z_0$, with the addition of a hard core repulsion δ_ϵ with ϵ equal to one pixel, producing configuration $\omega \in \Omega_C$;
   b) Evolve every circle in ω using gradient descent, with gradient field given by equation (9), until convergence, producing configuration $\tilde{\omega} \in \Omega_{\Gamma_o}$; and add the obtained elements to the current

configuration (which is empty at the first step);

3) **Death**
   a) For computational efficiency, sort the components of the current configuration w.r.t. their energy $H_1(\omega_i) = E(\tilde{\omega}_i)$;
   b) Remove each component ω_i independently from the current configuration with probability

   $$p_d(\omega_i, \omega) = \frac{\delta d_\beta(\omega_i, \omega)}{1 + \delta d_\beta(\omega_i, \omega)} ,$$

   where

   $$d_\beta(\omega_i, \omega) = e^{-\beta \Delta_i H(\omega)} ; \tag{14}$$

4) **Termination**
   If all the components added in the birth step are removed in the following death step, then stop; if not, then decrease the temperature $T = \frac{1}{\beta}$ and time step δ, (we use a geometric annealing schedule to T and δ), and go to the birth step.

IV. Experimental results

Figures 1 and 2 show the results of experiments on one band of a very high resolution colour infra-red (CIR) aerial image. The images show the top part of the tree crowns. The image viewpoint is close to the nadir, *i.e.* the tree crowns are seen from almost vertically above.

Figure 1 demonstrates the results of object extraction obtained using three different models. The top right image shows the configuration obtained using simply-shaped objects, in this case ellipses. The bottom left image shows the configuration obtained using the representation and energy described in this paper, but with no strong shape information, *i.e.* with $E_{\mathrm{sh}} \equiv 0$, or equivalently, $g \equiv 0$. The bottom right image shows the result obtained using the full energy described in this paper, *i.e.* with strong prior shape information included.

Note that for all three experiments there is no curve initialization, *i.e.* the initial configuration is empty. The first birth step creates a certain number of curves depending only on the Poisson mean z_0, but the final number is determined automatically by the convergence of the annealed birth-and-death process.

For the third experiment, the function $g(k)$ is defined so as to discourage low frequencies, and in particular $k = 2$, in order to avoid the extraction of two overlapping trees as a single elongated object, as well as to favour roughly circular objects with small perturbations corresponding to branches or leaves. The strong shape information allows us to extract nearby and even overlapping objects without paying the price of greatly simplifying their geometry.

Figure 2 shows the result of an experiment on another, bigger image of 900x900 pixels using the same model parameters as for the third experiment in figure 1. The image contains many overlapping tree crowns, but they are separated into distinct objects thus allowing delineation of the individual
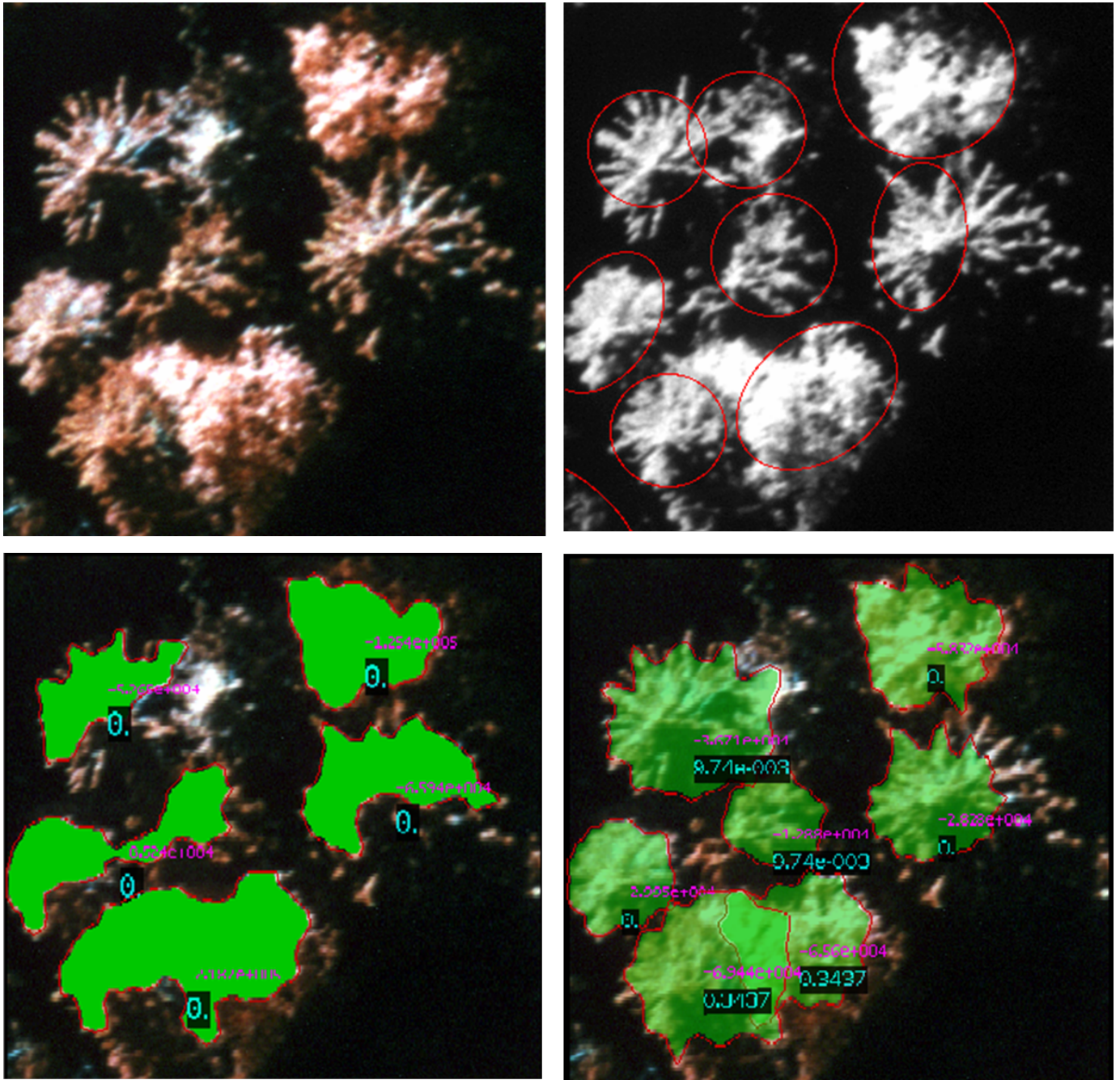
Fig. 1. Top, left: original CIR image of tree crowns, ©CBA. Top, right: final configuration using ellipse-shaped objects. Bottom, left: final configuration using arbitrarily-shaped objects obtained using an MPP without shape prior. Bottom, right: final configuration of arbitrarily-shaped objects obtained using an MPP with shape prior. The numbers show the interaction term value H_2 (black background) and the data term value H_1.

crowns. The computation time of the C++ programme was 25mn on a 2.16GHz processor.

To summarize, an MPP model using simply shaped marks allows the rapid detection of the objects in an image, but the geometrical accuracy is very low for objects with complex shapes. Therefore, this type of model is an appropriate tool for the detection of objects in low resolution images. The second approach, an MPP model for the extraction of arbitrarily-shaped objects with only weak shape information [10], is geometrically far more accurate, while not increasing the computational complexity unduly. The limitations of this approach, however, are that because it uses only weak shape information to define the possible single objects, it cannot, first, detect different types of objects with similar radiometric characteristics; and second, separate two or more overlapping objects. The MPP model for arbitrarily-shaped objects including strong prior shape information described in this paper deals with both these limitations. For example, in the bottom left corner of the bottom left image figure 1, there are two overlapping tree crowns that are extracted as one object using the second approach, but which are extracted as two distinct overlapping objects using the model presented in this paper. Using strong prior shape information has another advantage: even if the object to be extracted is partly obscured or cluttered, by, for example, shadow, like the spiky crowns of spruce trees, the object may nevertheless, to some degree of accuracy, be correctly extracted as a single object.

V. Conclusion and perspectives

The marked point process framework with simple geometries that has been used in the past for the extraction of objects from images has been recently extended to arbitrarily shaped objects. In this paper, we extend this approach further by incorporating strong prior knowledge about the shape of the objects sought, without increasing the dimensionality of the single-object space (and thereby the computational complexity). The set of possible single objects is defined using the local minima of an energy that incorporates information coming from the data and strong prior shape information about the objects sought. This allows us to deal with configurations of overlapping objects with complex shapes.

The birth-and-death algorithm used to minimize the multiple-object energy over configurations of multiple objects has the advantage that, at every iteration, the current configuration is updated by adding multiple objects independently of the current energy and temperature, which increases the computational efficiency.

The work in this paper can also be seen as the first step in a joint tree extraction and classification algorithm. For the class of images used in our experiments, once the tree crowns are extracted, one can then classify them into species [9].

The next step consists in further extending the model to the extraction of objects of several classes in scenes of high complexity containing overlapping, arbitrarily-shaped objects.

References

[1] Caselles, V., Kimmel, R., Sapiro, G.: Geodesic active contours. Int. J. of. Comp. Vis., (1997) **22(1)** : 61-79

[2] Cremers, D., Tischaeuser, F, Weickert, J., Schoerr, C.: Diffusion snakes: introducing statistical shape knowledge into the Mumford-Shah functional. Int. J. of Comp. Vis., (2002) **50(3)**: 295-313

[3] Cremers, D., Sochen, N., Schnörr, C.: A multiphase dynamic labeling model for variational recognition-driven image segmentation. Int. J. of Comp. Vis., (2006) **66(1)**: 67–81

[4] Cremers, D., Osher, S.J., Soatto, S.: Kernel density estimation space and intrinsic alignment for shape priors in level set segmentation. Int. J. of Comp. Vis., (2006) **69(3)**: 335–351

[5] Descombes, X., Minlos, R., Zhizhina, E.: Object extraction using a stochastic birth-and-death dynamics in continuum. J. Math. Imaging Vis., (2009) **33(3)**: 347–359

[6] Joshi, S. H., Srivastava, A.: Intrinsic Bayesien active contour for extraction of object boundaries in images. Int. J. of Comp. Vis., (2009) **81**: 331–355

[7] Juan, O., Keriven, R., Postelnicu, G.: Stochastic Motion and the Level Set Method in Computer Vision: Stochastic Active Contours. Int. J. of Comp. Vis., (2006) **69(1)**: 7–25

[8] Kass, M., Wiktkin, A., Terzopolous, D.: Shakes: Active contours models. Int. J. of Comp. Vis., (1998) **1(4)**: 321–331

[9] Kulikova, M., Mani, M., Srivastava A., Descombes, X., Zerubia, J.: Tree species classification using radiometry, texture and shape based features. Europ. Sign. Proc. Conf., (2007)

[10] Kulikova, M., Descombes, X., Jermyn, I., Zerubia, J., Zhizhina, E.: Extraction of arbitrarily-shaped objects using stochastic multiple birth-and-death dynamics and active contours. To be published in SPIE Electronic Imaging Proc. Conf., (2010)

[11] Lacoste, C., Descombes, X., Zerubia, J.: Point processes for unsupervised line network extraction in remote sensing. IEEE Trans. on Patt. Anal. and Machine Intel., (2005) **27(10)**: 1568–1579

[12] Leventon, M.E., Grimson, W.E.L., Fougeras, O.: Statistical shape influence in geodesic active contours. In Proc. Conf. Comp. Vis. and Patt. Recog., (2000): vol.1 316–323

[13] Ortner, M., Descombes, X., Zerubia. J.: Building outline extraction from digital elevation models using marked point processes. Int. J. of Comp. Vis., (2007) **72(2)**: 107–132

[14] Osher, S., Fedkiw, R.: Level Set Methods and Dynamic Implicit Surfaces. Springer Verlag (2003)

[15] Perrin, G., Descombes, X., Zerubia, J.: A marked point process model for tree crown extraction in plantation. In Proc. IEEE ICIP, (2005)

[16] Sethian, J.A.: Level Set Methods and Fast Marching Methods. Cambridge Univ. Press (1999)

[17] Srivastava, A., Jermyn, I. H.: Looking for Shapes in Two-Dimensional Cluttered Point Clouds. IEEE Trans. on Patt. Anal. and Machine Intel., (2009) **31(9)**: 1616–1629

[18] Storvik, G.: A Bayesian approach to dynamic contours through stochastic sampling and simulated annealing. IEEE Trans. on Patt. Anal. and Machine Intel., (1994) **16(10)**: 976–986

[19] Tu, Z., Zhu, S-C.: Image Segmentation by data-driven Markov Chain Monte Carlo. IEEE Trans. on Patt. Anal. and Machine Intel., (2002) **24(5)**: 657–673
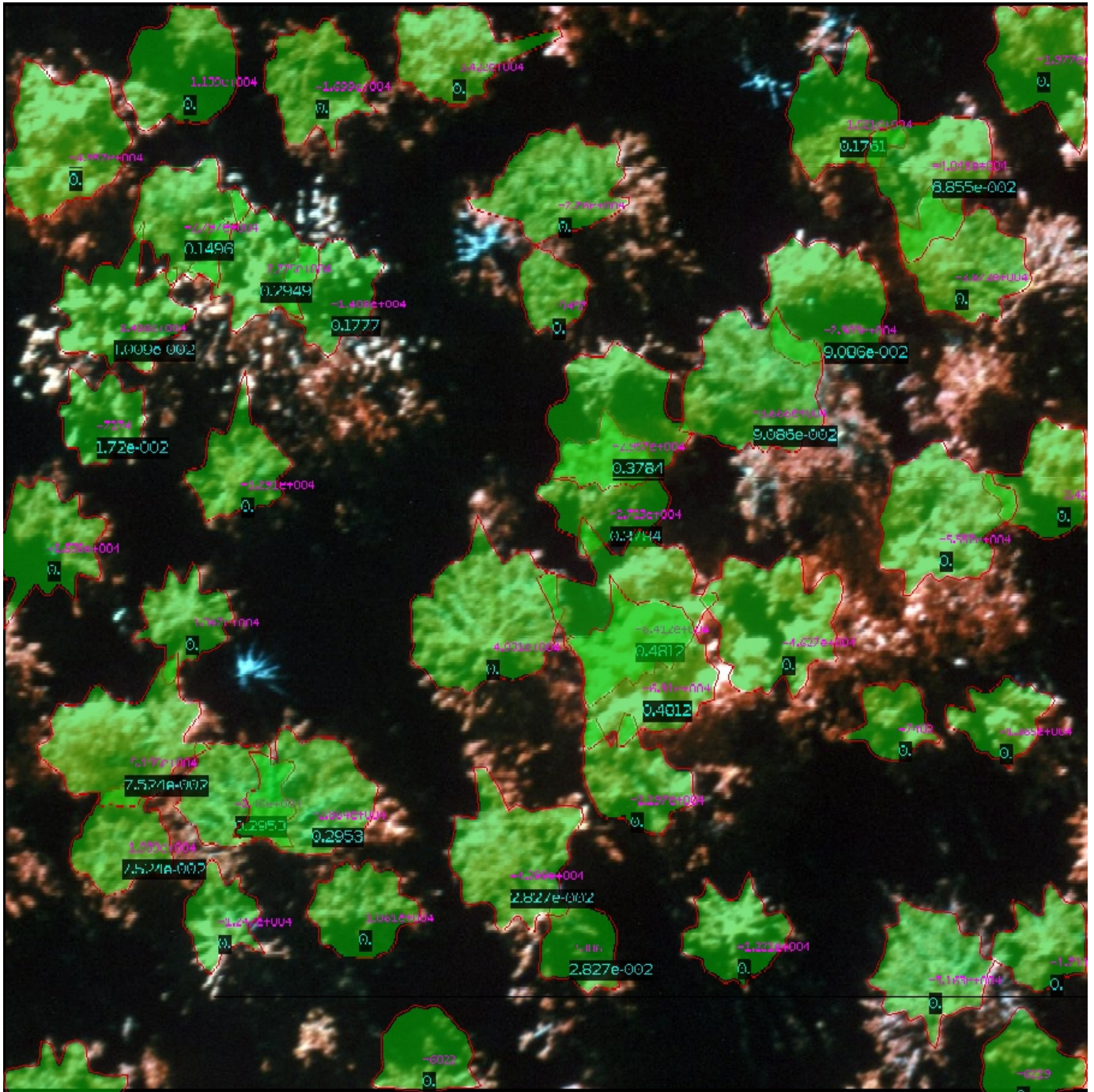
Fig. 2. Final configuration of arbitrarily-shaped objects obtained using an MPP with shape prior. The numbers show the interaction term value H_2 (black background) and the data term value H_1. Original image is a CIR of tree crowns, ©CBA.